Jpn. J. Appl. Phys. Vol. 32 (1993) pp. 989–995
Part 1, No. 2, February 1993

Magnetooptical Kerr Spectrometer for 1.2–5.9 eV Region and its Application to FePt/Pt Multilayers

Katsuaki SATO, Hidetoshi HONGU*, Hiroshi IKEKAME, Yasuhiro TOSAKA, Masato WATANABE[1], Koki TAKANASHI[2] and Hiroyasu FUJIMORI[2]

Faculty of Technology, Tokyo University of Agriculture and Technology, Koganei, Tokyo 184
[1]*The Research Institute for Electric and Magnetic Materials, Taihaku-ku, Sendai 982*
[2]*Institute for Materials Research, Tohoku University, Katahira, Aoba-ku, Sendai 980*

(Received September 26, 1992; accepted for publication November 21, 1992)

The apparatus for measurement of magnetooptical spectra using a polarization modulation technique has been improved to extend the short-wavelength limit to about 200 nm in the ultraviolet range. Short-wavelength characteristics of the light source, the focusing system including mirrors and lenses, the monochromator, the polarizer and the analyzer were improved. The techniques of calibration for Kerr rotation and ellipticity were also refined. With the use of the newly designed system, the magnetooptical Kerr rotation and Kerr ellipticity of FePt/Pt multilayers, as well as of FePt alloys of different compositions were evaluated for photon energies between 1.2 and 5.9 eV.

KEYWORDS: magnetooptical spectrum, ultraviolet wavelength, Kerr rotation, Kerr ellipticity, polarization modulation technique, Rochon prism, FePt/Pt multilayer

1. Introduction

There have been rapid developments in the field of magnetooptical (MO) recording in recent years[1)] and research for higher density MO recording with short-wavelength laser light has been ongoing. For this purpose, a number of studies of the periodic structure of ultrathin films, such as Co/Pt and Fe/Pt multilayers have been attempted, because they show a large MO effect in the short-wavelength region around 300 nm.[2-4)] However, only a few studies have been conducted on the physical origin of MO effects in these multilayers. In order to obtain an insight of the electronic structures which cause the short-wavelength MO effect, it is necessary to investigate MO spectra for a wide range of photon energies. In particular, information on Kerr ellipticity, which is crucial for the detailed analysis of MO spectra, is lacking for most of the reported MO spectra in multilayers.

The wavelength region of measurement in previous magnetooptical spectrometers has been limited to wavelengths not less than 250 nm for several technical reasons. In addition, no conventional equipment reported to date allows the measurement of both rotation and ellipticity to cover the wavelength region below 250 nm.

By means of a polarization modulation technique with a photoelastic modulator,[5)] we have obtained MO Kerr spectra in diverse materials,[6-8)] providing both rotation and ellipticity for a considerably wide wavelength region between 0.5 eV (~2.5 μm) and 3.0 eV (~400 nm). Since the short-wavelength limit of 400 nm was determined by the spectral properties of optical elements used in the system, we have made improvements in all the elements of the apparatus and have constructed a new system to measure MO spectra for the photon energy region between 1.2 eV (~1000 nm) and 5.9 eV (~210 nm).

We have also improved the calibration technique for both rotation and ellipticity. We propose a new method which provides calibrated values more directly than previous methods.

With the use of the newly constructed MO apparatus, MO spectra in FePt/Pt multilayers and FePt alloys prepared by the ion-beam sputtering were evaluated for the first time between 1.2 and 5.9 eV. In the present paper, only the experimental data are described. Detailed analyses will be given elsewhere.

2. Principles of the Technique

The principle of measurement of magnetooptical Kerr rotation and Kerr ellipticity spectra is based on the use of the polarization modulation technique employing a photoelastic modulator. In this section, we briefly summarize the technique described by one of the authors (K. S.) in ref. 5.

A schematical illustration of the apparatus is shown in Fig. 1, which is essentially the same as that described in ref. 5. Light from a monochromator is polarized linearly by a polarizer with the transmission axis forming an angle of 45° with the vertical and modulated by a photoelastic modulator (Hinds Inc., PEM-CF3). The modulator causes retardation expressed by the formula

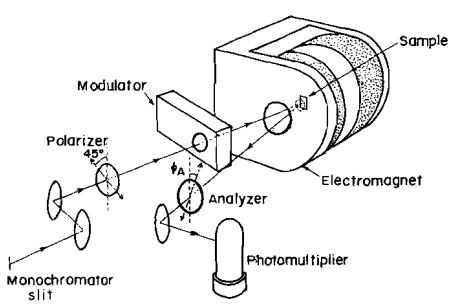

Fig. 1. A schematical illustration of the polarization modulation technique described in ref. 5.

*Present address: Sumitomo Electric Works Ltd., Yokohama 244.

$$\delta=\delta_0 \sin 2\pi pt, \tag{1}$$

between vertical and horizontal polarizations, where δ_0 denotes the amplitude of retardation and p the modulation frequency. The retardation amplitude δ_0 is kept constant by applying the wavelength-proportional voltage to the modulator control. Modulated light is reflected by a magnetized sample situated at the focal point of the mirror system and is passed through an analyzer with the transmission axis forming an angle of Φ_A to the vertical and is detected by a photomultiplier.

As derived in ref. 5, the intensity I of light detected by the photomultiplier is represented by

$$I=I_0\{R+(\Delta R/2)\sin\delta+R\sin(\Delta\theta+2\Phi_A)\cos\delta\}. \tag{2}$$

This expression can be rewritten as

$$I=I(0)+I(p)\sin 2\pi pt+I(2p)\cos 4\pi pt+\cdots, \tag{3}$$

where the DC-component $I(0)$, p Hz-component $I(p)$ and $2p$ Hz-component $I(2p)$ are expressed as follows:

$$I(0)=I_0R\{1+J_0(\delta_0)\sin(\Delta\theta+2\Phi_A)\}, \tag{4}$$

$$I(p)=I_0\Delta RJ_1(\delta_0), \tag{5}$$

$$I(2p)=2I_0RJ_2(\delta_0)\sin(\Delta\theta+2\Phi_A), \tag{6}$$

$J_n(x)$ denoting n-th order Bessel functions.

We denote the amplifier output for DC-, p Hz- and $2p$ Hz-components as I_0, I_p and I_{2p}, respectively. The ratios of I_p/I_0 and I_{2p}/I_0 are expressed in the case of $\Phi_A=0°$ as

$$I_p/I_0=AJ_1(\delta_0)\Delta R/R, \tag{7}$$

$$I_{2p}/I_0=BJ_2(\delta_0)2\Delta\theta, \tag{8}$$

as long as $\Delta\theta$ is sufficiently small and the second term in eq. (4) can be neglected. Here A and B denote appropriate parameters representing the ratio of gains of the detector-amplifier system for p Hz- and $2p$ Hz-components to the DC-component, respectively.

Since Kerr rotation θ_K and Kerr ellipticity η_K can be expressed respectively, in terms of $\Delta\theta$ and $\Delta R/R$ by the formulae

$$\Delta\theta=-2\theta_K, \tag{9}$$

$$\Delta R/R=4\eta_K, \tag{10}$$

eqs. (7) and (8) can be rewritten as

$$I_p/I_0=4AJ_1(\delta_0)\eta_K, \tag{7'}$$

$$I_{2p}/I_0=-4BJ_2(\delta_0)\theta_K. \tag{8'}$$

We can obtain Kerr ellipticity and Kerr rotation from eqs. (7') and (8') provided that $AJ_1(\delta_0)$ and $BJ_2(\delta_0)$ have been determined. Calibration methods for determining the values of $AJ_1(\delta_0)$ and $BJ_2(\delta_0)$ will be described in §5.

In a conventional magnetooptical spectrometer, a quarter-wave plate for appropriate wavelength is necessary for determining ellipticity. Therefore several different quarter-wave plates should be prepared to obtain the ellipticity spectra for a wide range of wavelengths. On the other hand, our system provides information for both rotation and ellipticity for a vast wavelength region, if the modulation amplitude of the photoelastic modulator is controlled to assure constant retardation by application of a suitable voltage corresponding to wavelength.

3. Improvement of the System

In this section we describe several improvements made to extend the wavelength region of measurement.

3.1 *Light source*

We used a Xe lamp (Hamamatsu, type L2175) made of fused silica, instead of the ozoneless Xe lamp in the previous system. Although the specifications state that the shortest ultraviolet wavelength of the lamp is 185 nm, the practical limit was 200 nm, for obtaining sufficient intensity for MO measurements. We adopted a lens made of composed silica for focusing the Xe light onto the entrance slit of the monochromator, which assures 90% transmission at 200 nm.

3.2 *Monochromator*

We used a double monochromator (JASCO, type CT-25CD) instead of the single monochromator (JASCO, type CT-25C) employed in the previous system in order to reduce stray light, which often has a serious effect on the ultraviolet MO spectrum giving rise to incorrect spectral shape, since the total intensity of visible light from the Xe lamp is stronger than ultraviolet light by several orders of magnitude. By adoption of the double monochromator, stray light was reduced to a negligible level. A 1200 groove/mm grating blazed at 200 nm was adopted to ensure high efficiency in the ultraviolet region.

The slit width of 1.5 mm for both entrance and exit slits was necessary to ensure a sufficient signal-to-noise ratio (SNR) for measurement at the shortest wavelength (210 nm). This corresponds to a resolution of 0.05 eV at 6 eV and 0.01 eV at 4 eV.

3.3 *Polarizers*

In our system two polarizers were necessary, one in front of the modulator and the other behind the sample. In the previous system, we used Glan-Foucault prisms (Halle Inc.) made of calcite. However, the transmittance of calcite dropped gradually from 400 nm towards shorter wavelengths, decreased steeply below 270 nm and became less than 10% at 240 nm. Therefore, the practical wavelength limit of this polarizer was actually 250 nm.

For wavelengths shorter than 250 nm, we adopted a Rochon prism polarizer made of MgF_2, which showed transmittance as high as 85% at 200 nm and a fairly good extinction ratio of 49 dB at 1.3 μm.

Despite good short-wavelength characteristics, the Rochon prism has a drawback which required special care in the design of a system: it gives double images, i.e., it transmitted both ordinary and extraordinary light with an angle of separation as small as 3° between the two beams.

3.4 *Focusing optics with ellipsoidal mirrors*

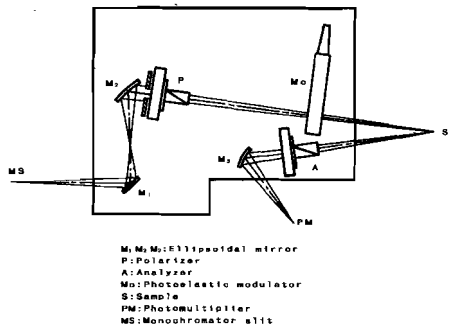

Fig. 2. A schematical illustration showing the arrangement of optical elements.

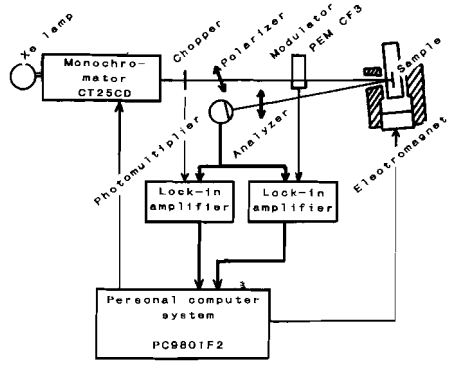

Fig. 3. A block diagram of the newly designed MO spectrometer.

The focusing optics of the newly designed system is illustrated in Fig. 2. To avoid the problems of absorption and chromatic aberration, we used ellipsoidal mirrors (M_1, M_2 and M_3) of evaporated aluminium coated with MgF_2 protective film as focusing elements. The thickness of the coating was carefully determined so as to yield high reflectivity at a short wavelength. Since the placement of any focussing elements between PEM and analyzer causes false signals of rotation or ellipticity we used an ellipsoidal mirror with a long focal length for mirror M_2.

Special care was taken in the design of the optical system to use the Rochon prisms as polarizers. First, to ensure a sufficient separation between the two beams from the Rochon prism, it was necessary to maintain a sufficient distance between the prism P and the modulator Mo. However, as the distance increases, the required f-number of the ellipsoidal mirror increases, which in turn causes a decrease in the light intensity at the specimen. The second focal length of the ellipsoidal mirror M_2 was determined to be as long as 548 mm and the Rochon prism P was placed 90 mm from mirror M_2. Modulator Mo was placed at the distance of 190 mm from polarizer P, by which the separation of about 10 mm was obtained between the centers of the two beams. A mask was placed just before the modulator to screen the ordinary light. The same care was also taken with analyzer A (the second polarizer). Two beams emitted from analyzer A were focused using ellipsoidal mirror M_3 and were screened by a slit placed at the focal point just in front of the photomultiplier PM. In addition, the difference in the optical length due to insertion of the polarizer was also taken into account in the design of the optics, since the difference due to the Rochon prism employed was as large as 20 mm.

4. System of Measurement

Figure 3 shows a schematical illustration of our measuring system. The angle of incidence on the sample surface in this system was set at 7.5°, due to constraints in the layout of optical elements, especially the size of the modulator. Since the magnitude of the MO effect is proportional to the scalar product of the wave vector $\boldsymbol{k}$ and magnetization $\boldsymbol{M}$, the angle of incidence can be regarded as satisfying the condition of perpendicular incidence. Magnetooptical constants determined using this system, therefore, undergo a reduction due to the deviation from the normal incidence. Nevertheless, we can neglect this reduction, since cos 7.5° equals 0.991.

An electromagnet with a gap of 20 mm between pole pieces was employed to saturate the sample, the maximum field being 1 T. The magnet has a tapered perforation in one of the pole pieces, the diameter of the perforation at the inside wall being 8 mm and that at the outside wall being 60 mm. Prior to the measurement of MO spectra, Kerr hysteresis loops were measured to confirm that the magnetization of the sample was saturated by the applied magnetic field.

We used a photomultiplier (Hamamatsu R2658) with InGaAs photocathode to ensure measurements without changing the detector over wide range of wavelengths, since it covers wavelengths from 185 nm to 1000 nm. In order to avoid the effect of the leakage field from the electromagnet, the photomultiplier was covered by a specially designed permalloy shield.

The high-voltage supply for the photomultiplier was controlled by a feedback system to make the DC-component constant. Without such a system the spectrum obtained often shows an unreliable lineshape, since the photomultiplier response varies depending on the DC-photocurrent.

Extension of the wavelength beyond 1050 nm in the infrared region is possible by replacing the photomultiplier with a semiconductor photodiodes.

Our measuring system was equipped with a personal computer with an interface to control the magnetic fields, the wavelength of the monochromator, and the modulating amplitude of the PEM and to acquire the data from lock-in amplifiers.

The measured magnetooptical spectra usually show spurious signals of rotation and circular dichroism, which may be ascribed to the deviation of the angle of incidence from the normal incidence, as well as to the optical anisotropy inherent to the sample. We therefore measure the magnetooptical effect for both polarities of the magnetic field at each step of the wavelength scan and take the difference between the values for the two polarities of magnetic field.

5. Calibration

5.1 *Kerr rotation*

Calibration of Kerr rotation was attempted using

three methods. The first method is that described in ref. 5. The second involves calibration using a Faraday rotation cell. The third is a new technique which is proposed here.

First, the method described in ref. 5 is briefly summarized. Using a plane mirror at the sample position and setting the polarizing angle of the second polarizer at $\pm 45°$ to the vertical axis, we measure I_{2p}/I_0. In this case, substituting $\Phi_A = \pm 45°$ and $\Delta\theta = 0$ into eqs. (4) and (6) we obtain,

$$I_{2p}/I_0 = \pm 2BJ_2(\delta_0)/\{1 \pm J_0(\delta_0)\}, \tag{11}$$

the double sign corresponding to the sign of the polarizing angle. Thus we can determine the parameter $BJ_2(\delta_0)$ using the two values of I_{2p}/I_0 for $\pm 45°$.

In our previous studies, the parameter $BJ_2(\delta_0)$ thus calibrated was assumed constant over the wavelength range of measurements. However, measurement of the spectral variation revealed that although the value can be assumed constant from 1000 nm to about 400 nm, it shows a gradual decrease towards the shorter wavelengths. Therefore, it is found that the calibration should be performed over the entire range of measured wavelengths.

However, since this method requires a rotation of the analyzer angle as large as $\pm 45°$, a substantial change in measuring conditions is inevitable. Thus, the absolute value of the calibration constant is less reliable than that of the direct calibration technique which will be described later.

Next, we describe the Faraday cell method. By setting a mirror in place of the sample and setting a Faraday cell (HOYA, type M210) along the optical path, the value of rotation can be calculated directly from the current supplied to the Faraday rotator. According to the specifications of the cell, the angle of rotation is 2.2° per ampere at 633 nm. Calibration by this method provided a value in good agreement with that of the first method with an accuracy of about 1% at the wavelength specified.

Finally a new proposal of a direct calibration technique which provides a more reliable means for the determination of rotation angle is presented. We use a plane mirror at the sample position or keep the sample in the position of measurement and the polarization angle is adjusted to be nearly vertical where minimum output of $I(2p)$ is obtained. Then the analyzing angle is rotated from $+2°$ to $-2°$ by a step of 1.0° and the value of I_{2p}/I_0 is recorded. By taking the difference between the values for the analyzer angles of the same absolute values with different signs (*e.g.*, $+1°$ and $-1°$), the calibrated value per unit angle is obtained.

We explain the above-mentioned technique using mathematics. In this case, Kerr rotation of the sample $\Delta\theta$ is assumed nearly the same order of magnitude as that of the analyzer angle of $\Phi_A = \pm 1°$. In this case sin $(\Delta\theta + 2\Phi_A)$ in eq. (6) can be approximated by $\Delta\theta + 2\Phi_A$. Since the value is of the order of 0.02, $J_0(\delta_0)$ sin $(\Delta\theta + 2\Phi_A)$ in eq. (4) can be neglected, when compared with unity. By taking the difference between the signals for $\pm\Phi_A$ and dividing by $2\Phi_A$, we obtain

$$([I_{2p}/I_0]_{+\Phi_A} - [I_{2p}/I_0]_{-\Phi_A})/2\Phi_A = 4BJ_2(\delta_0), \tag{12}$$

which directly provides the calibration constant $4BJ_2(\delta_0)$ in eq. (8′).

This method allows direct calibration of Kerr rotation for the entire spectral range of measurement. The values (in radians units) of the parameter $BJ_2(\delta_0)$ calibrated by this method are shown as a function of the photon energy in Fig. 4 determined for two analyzer angles of 1° and 2°. The two curves show agreement within the accuracy of a few percent. The photon energy dependence of the value shows a perfect coincidence with that of $BJ_2(\delta_0)$ calibrated by the first method, although the absolute value differs by nearly 5% between the two methods.

5.2 *Kerr ellipticity*

As for the calibration of Kerr ellipticity, we used the method described in ref. 5. This calibration technique uses a quarter-wave plate and a mirror at the sample position. If we set the polarization angle at $\pm 45°$ to the vertical axis, the ratio I_p/I_0 is given as

$$I_p/I_0 = \mp 2AJ_1(\delta_0). \tag{13}$$

Due to the limitation of available quarter plates, calibration of the parameter $AJ_1(\delta_0)$ in eq. (11) was performed at 633, 488 and 250 nm.

In order to obtain a calibrated value of ellipticity for the entire spectral region, just as in the case of the Kerr rotation, the calibration method using a retardation plate made of sapphire[9] was applied. A sapphire crystal plate of 0.295 mm thickness was cut along the crystal plane which assures double refraction. If we set the optic axis of the sapphire plate in the vertical direction and the polarizing direction of the analyzer at $\pm 45°$, the spectral dependence of I_p/I_0 shows an oscillating spectral dependence, maxima and minima appearing at wavelengths where retardation becomes $\pm\pi/2$, the envelope providing a calibration function.

This technique can be explained mathematically as follows. In this setup, the retardation δ in eq. (2) should be replaced by

$$\delta = \delta_0 \sin 2\pi pt + \delta_s, \tag{14}$$

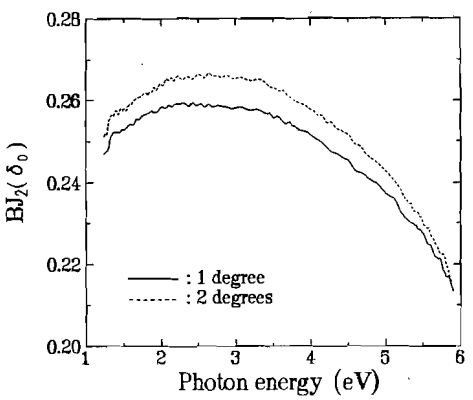

Fig. 4. Spectrum of the calibration parameter for rotation, $BJ_2(\delta_0)$ determined by the newly proposed technique determined with the analyzer angle Φ_A of 1° and 2° (see text).

where $\delta_s=2\pi ln/\lambda$ expresses retardation by the sapphire plate. Since the usual mirror does not show circular dichroism, the second term in eq. (2) vanishes. Then eq. (2) becomes

$$I=I_0R[1\pm J_0(\delta_0)\cos\delta_s\mp 2J_1(\delta_0)\sin\delta_s\sin 2\pi pt \mp 2J_2(\delta_0)\cos\delta_s\cos 4\pi pt]. \quad (15)$$

At the wavelength where retardation δ_s takes the value of $\pm\pi/2$, $\cos\delta_s$ vanishes and $\sin\delta_s$ takes the value of ± 1, thus the ratio of I_p/I_0 is given by the following formula,

$$I_p/I_0=\pm 2AJ_1(\delta_0). \quad (16)$$

The resulting spectrum of $\pm AJ_1(\delta_0)\sin\delta_s$ for the above-mentioned arrangement in our system is illustrated in Fig. 5, where straight and broken lines correspond to the analyzer angles of $+45°$ and $-45°$, respectively. Thin lines show the envelope functions providing $\pm AJ_1(\delta_0)$ which demonstrate a slight decrease with the increase in photon energy. The dependence may be ascribed to the inability in keeping the retardation amplitude δ_0 constant.

A similar direct calibration technique as proposed for the calibration of Kerr rotation can be applied to ellipticity. We use a plane mirror at the sample position or keep the sample as it is at the measuring position and the quarter-wave plate is inserted with its optic axis parallel to the vertical direction. Then the analyzing angle Φ_A is varied stepwise between $+2°$ and $-2°$ and we record I_p/I_0. If we take the difference between the values for $\pm\Phi_A$ and divide by $2\Phi_A$, the calibration signal per unit angle of ellipticity can be obtained.

In this case, eq. (2) becomes

$$I=I_0\{R-(\Delta R/2)\cos(\delta_0\sin 2\pi pt)+R\sin(\Delta\theta+2\Phi_A)\times\sin(\delta_0\sin 2\pi pt)\}. \quad (17)$$

Then $[I_p/I_0]_{\pm\Phi_A}$ can be approximated as

$$I_p/I_0=2AJ_1(\delta_0)(\Delta\theta\pm 2\Phi_A). \quad (18)$$

Therefore

$$([I_p/I_0]_{+\Phi_A}-[I_p/I_0]_{-\Phi_A})/2\Phi_A=4AJ_1(\delta_0) \quad (19)$$

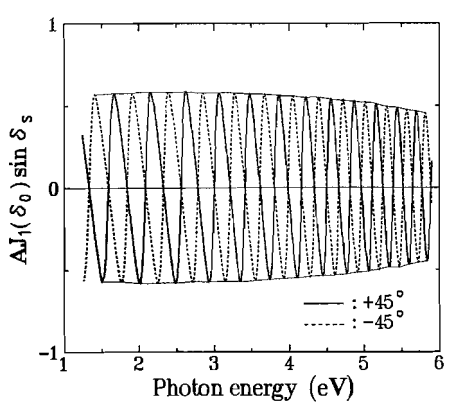

Fig. 5. Spectrum of the calibration parameter for ellipticity, $AJ_1(\delta_0)\sin\delta_s$ determined using a sapphire plate, where solid and broken lines correspond to analyzer angles of $+45°$ and $-45°$, respectively. The envelope functions shown by thin solid lines are for $\pm AJ_1(\delta_0)$ (see text).

provides the direct evaluation of the coefficient $4AJ_1(\delta_0)$ in eq. (7′). The value thus determined was identical to that obtained using the sapphire technique within the accuracy of $\pm 2\%$.

If the quarter-wave plate is replaced by a sapphire retardation plate, the calibration value can be obtained from the envelope function for entire range of photon energies.

5.3 *Sign convention*

In this work, we adopt a sign convention defined as follows. The magnetic field is set parallel to the direction of light propagation and the rotation is taken as positive when the reflected beam undergoes a clockwise rotation from the incident linear polarization viewed by an observer facing the sample. The polarity of the Kerr ellipticity is assumed to become consistent with that obtained by the Kramers-Kronig analysis of the rotation by the following formula.[10]

$$\eta_K(\omega)=-(2\omega/\pi)\mathscr{P}\int_0^\infty\{\theta_K/(x^2-\omega^2)\}\,dx, \quad (19)$$

where $\mathscr{P}$ stands for the principal part of integration.

6. Examples-Magnetooptical Spectra of FePt/Pt Multilayers

We have been measuring MO spectra in multilayers using the newly designed spectrometer. We have previously published the results of spectra of Co/Pt and Fe/Pt multilayers elsewhere.[11] Here we show results of MO spectra measurement in FePt/Pt multilayers.

FePt/Pt multilayers were prepared by an ion-beam sputtering technique through the Pt buffer layer on the MgO(100) crystal.[12] The FePt layer thickness x of the sample was varied from 20 Å to 200 Å, keeping the Pt layer thickness at 50 Å. The surface layer of each sample is a FePt layer in all cases.

The total thickness of the multilayers was kept at approximately 2000 Å (between 1500 and 2700 Å); thus the number of layers N_L differ from sample to sample: N_L was 5, 10, 13, 20, 28 and 35 for FePt thickness x of 200, 100, 75, 50, 35 and 20, respectively.

Kerr rotation and ellipticity spectra from 1.2 to 5.9 eV in the above-mentioned FePt(x Å)/Pt(50 Å) samples measured using the newly constructed system are shown in Figs. 6(a) and 6(b), respectively. The sample with the thickest FePt layer, $x=200$ Å, shows a peak at 4.7 eV, the maximum value being 47 min of arc. On the other hand, the Kerr ellipticity spectra show the maximum at the highest photon energy. The maximum value reaches to nearly 80 min of arc at 5.9 eV.

As the FePt thickness x decreases the peak energy position of Kerr rotation spectra moves towards high energies and the peak rotation decreases. For $x=50$ Å, the peak occurs at 5.2 eV. At this composition ratio, X-ray diffraction provides no periodic structure.[13] For x less than 50 Å, periodic structure is recovered and spectral features undergo clear changes. The minimum position is subject to abrupt change at the thickness of 50 Å: it is fixed at 2.7 eV for $x>50$ Å while it moves towards low energies for $x<50$ Å. Such structural tran-

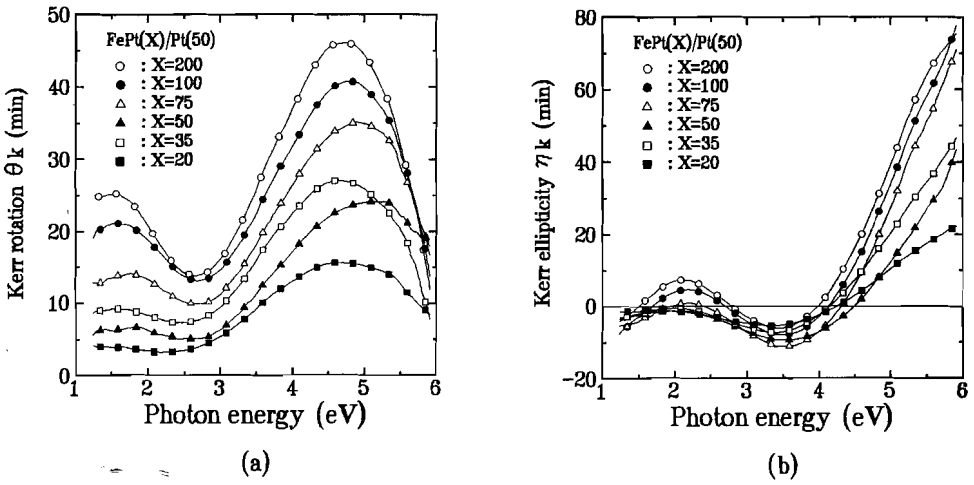

Fig. 6. MO spectra of FePt(x Å)/Pt(50 Å) multilayers between 1.2 and 5.9 eV. (a) Kerr rotation and (b) Kerr ellipticity.

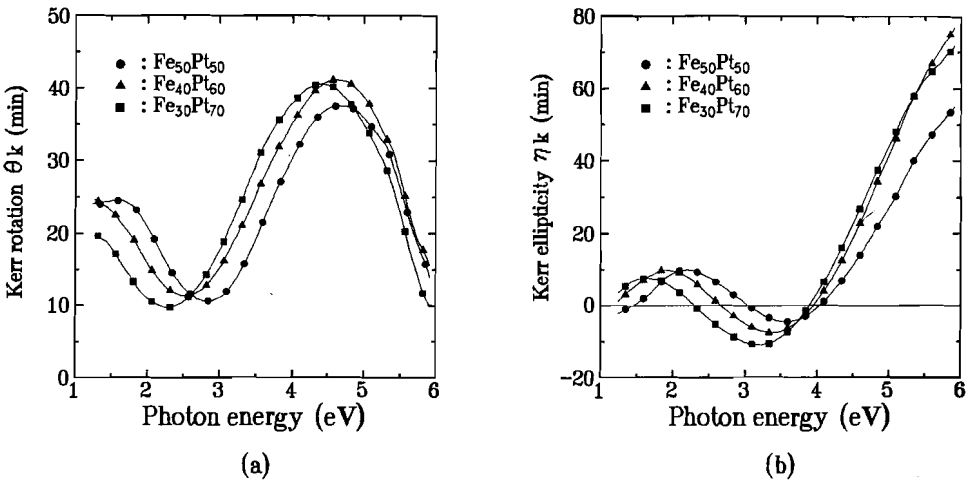

Fig. 7. MO spectra of Fe_xPt_{100-x} (x=50, 40 and 30 Å) alloys between 1.2 and 5.9 eV. (a) Kerr rotation and (b) Kerr ellipticity.

sition at the thickness can be more easily observed in Kerr ellipticity spectra, in which three curves with x=200, 100 and 75 Å and those with x=35 and 20 Å show different spectral behavior especially in the low energy region. These results show that the structural transition is accompanied by the change in electronic structures.

The MO spectra for three alloy samples with different composition ratios, i.e., $Fe_{50}Pt_{50}$, $Fe_{40}Pt_{60}$ and $Fe_{30}Pt_{70}$, are also given in Figs. 7(a) and 7(b). It is elucidated that in Fe_xPt_{100-x} the spectrum shows a low-energy shift as x is reduced from 50 to 30. The overall shape of the MO spectrum in the FePt(200)/Pt(50) multilayer is revealed to be identical to that of $Fe_{40}Pt_{60}$. Detailed analyses of the MO spectra in FePt/Pt multilayers will be described in later publications.

7. Conclusions

We have constructed a spectrometer to measure the magnetooptical Kerr rotation and ellipticity for a wide range of wavelengths from 1.2 to 5.9 eV. Special attention was paid to extend the range of measured wavelengths to the ultraviolet region. Using the apparatus we obtained magnetooptical spectra in FePt/Pt multilayers for a wide range of photon energies.

Acknowledgments

This work has been supported in part by a Grant-in-Aid for Scientific Research in Priority Areas from the Ministry of Education, Science and Culture. We also express sincere gratitude to Pioneer Ltd. and Mitsui Petrochemical Industries Ltd. for financial support. Thanks are also due to Yamada Optical Industries Ltd. for construction of focusing optics, to Nippon Kagaku Engineering Ltd. for construction of the electromagnet, and to Kogaku-Giken Ltd. for designing the Rochon prism polarizers and the sapphire plate.

1) M. H. Kryder: *Proc. Magneto-Optical Recording Symposium '90, Tokyo, April 1991*, J. Magn. Soc. Jpn. **15** (1991) Suppl. S1, p. 139.
2) P. F. Carcia, A. D. Meinhadt and S. Suna: Appl. Phys. Lett. **47** (1985) 178.
3) W. B. Zeper, F. J. A. M. Greidanus and P. F. Carcia: IEEE

Trans. Magn. **25** (1989) 3764.
4) S. Hashimoto and Y. Ochiai: J. Magn. & Magn. Mater. **88** (1990) 211.
5) K. Sato: Jpn. J. Appl. Phys. **20** (1981) 2403.
6) K. Sato, H. Kida and T. Kamimura: *Proc. Int. Symposium Magneto-Optics, Kyoto, April 1987*, J. Magn. Soc. Jpn. **11** (1987) Suppl., S1, p. 113.
7) K. Sato, Y. Aman and M. Hirai: *Proc. Int. Conf. Magnetism '88, Paris, August 1988*, J. Phys. (France) **49** (1988) Suppl. C8, p. 213.
8) K. Takanashi, K. Sato, J. Watanabe, Y. Sato and H. Fujimori: Jpn. J. Appl. Phys. **30** (1991) 52.
9) G. A. Osborne, J. C. Cheng and P. J. Stephans: Rev. Sci. Instrum. **44** (1973) 10.
10) D. Y. Smith: J. Opt. Soc. Amer. **66** (1970) 547.
11) K. Sato, H. Hongu, H. Ikekame, J. Watanabe, K. Tsuzukiyama and Y. Togami: Jpn. J. Appl. Phys. **31** (1992) 3603.
12) M. Watanabe, K. Takanashi and H. Fujimori: J. Magn. Soc. Jpn. **15** (1991) 415 [in Japanese].
13) M. Watanabe, K. Takanashi and H. Fujimori: J. Magn. & Magn. Mater. **113** (1991) 110.